Islamic Azad University
Mashhad Branch

Ashrafi and Hajalilou / Iranian Journal of Earth Sciences 9 (2017) / 48-63

Geochemistry of the Paleocene Sediments from SW Ahar: Implications for Provenance, Tectonics and Source Rock Weathering

Nasser Ashrafi [*1], Behzad Hajalilou[2]

Department of Geology, Payame Noor University, P.O. Box 19395-3697 Tehran, Iran

Received 11 April 2016; accepted 23 October 2016

Abstract

The mineralogy and geochemistry of Paleocene shales and interbedded siltstones in the southwestern part of Ahar town (NW Iran) were studied by optical microscopy, x-ray diffractometry (XRD), scanning electron microscopy (SEM), x-ray fluorescence (XRF), and inductively coupled plasma mass spectrometry (ICP-MS) techniques. The mineralogical composition, mainly characterized by calcite, quartz, feldspar, dolomite, muscovite, magnesiohornblende, chlorite, illite, montmorionite, palygorskite, and koninckite, suggests relatively fast erosion of the parent rocks and incipient metamorphism for the studied sediments. The values of weathering indices and the Index of Compositional Variability, as well the mineralogy of the sediments imply moderate weathering in the parent rocks and deposition as first cycle sediments. The shales exhibit higher Al_2O_3/TiO_2 (≈21), La/Sc, and Th/Cr values corresponding to felsic and/or intermediate source rocks. The geochemical character of sediments, including ∑REE=116 ppm, (La/Yb)N=8.3, (Eu/Eu*)=0.78, and the values of immobile elemental ratios suggest an immature continental arc setting. The typical shale and chondrite normalized REE patterns of the shales are comparable with continental arc terrigenous sediments and Andean-type andesites. The inferred tectonic setting for the studied shale is in concordance with the tectonic evolutionary history of NW Iran, during the Upper Cretaceous-Upper Paleocene. According to the present data, it can be concluded that the ultimate provenance of the studied shale and its interbedded siltstone and thin detritic limestone is probably the Upper Cretaceous sediments with the geoenvironment of acidic to intermediate volcanic rocks and marl.

Keywords: *SEM-EDX analysis, shale, interbedded siltstone, Neo-Tethyan subduction, Goouradaraq*

1. Introduction

A wide range of techniques exist for determining the ultimate source of the constituents in a mudrock. Stratigraphic, petrographic, mineralogic, and chemical techniques aid in determining the provenance of both the mudstone and its interbedded siltstones and sandstones. Most of the provenance studies of mudstones utilize chemical methods which are accompanied by petrographic study of the companion sandstones and siltstones (Bhatia and Crook 1986; Roser and Korsch 1986, 1988; Taylor and McLennan 1991; McLennan et al. 1993; Fedo et al. 1996; Hassan et al. 1999; Cullers 2000; Paikaray et al. 2008; Gosh and Sarkar 2010; Cao et al. 2012). Major element chemistry is possibly best employed in determining the extent of weathering of the source terrain (Nesbitt and Young 1982, 1984; Harnois 1988; Fedo et al. 1995). The most important elements to identify the sedimentary provenance and particular geochemical processes are the rare earth elements (REE), thorium (Th), scandium (Sc), and to a lesser extent chromium (Cr) and cobalt (Co) (Fleet 1984; Bhatia and Crook 1986; Cullers et al. 1988; McLennan 1989) because they have very low concentrations in sea and river waters, low residence times in the ocean and element ratios which are unaffected by diagenesis and metamorphism (Rollinson 1993). Thus, they are transported exclusively in the terrigenous component of sediment and reflect the chemistry of their source. Clay minerals typically have much higher total REE concentrations than coarser size-fractions (Cullers et al. 1987), and appear to be the most important mineral fraction in hosting REE in mudstones (Condie 1991). In general, mud derived from continental crust (with or without a superimposed volcanic arc) is LREE enriched, and has high ∑REE compared to mud deposited adjacent to juvenile arcs (McLennan et al. 1990).

This study describes the geochemistry of the major, trace, and rare earth elements of the Upper Paleocene shales from SW Ahar, NW Iran, and discusses the inferred source rocks, paleoweathering pattern and paleotectonics. The study also compares the major and trace element contents of the studied shale with their counterparts in other regions of the world. This is the first study which presents a mineralogical, major and trace element data for the sediments of SW Ahar.

---

*Corresponding author.
E-mail address (es): n_ashrafi@pnu.ac.ir

2. Geology

The subduction of Neo-Tethys beneath the Central Iran plate during the Upper Cretaceous to Paleogene and following the collision of Iranian and Arabian plate is known as the continent–continent collision and is responsible for the development of three ribbon structural zones in Iran (Fig 1). These SE trending structural zones include the Zagros folded-thrust belt, Sanandaj–Sirjan metamorphic zone, and Urumieh-Dokhtar magmatic arc (UDMA) (Stocklin and Nabavi 1973; Dewey et al. 1973; Sengor 1984; Jackson and McKenzie 1984; Alavi 1991; Alavi 2004). The NW-trending Alborz-Azarbaijan magmatic belt (AAMB) that stretches from the Alborz Mountains to Azarbaijan Province is separated from the UDMA to the south by the Tabriz Fault. Magmatic activity in UDMA and AAMB (as active continental margin) was initiated in the Late Cretaceous and continued during Eocene until the Quaternary period. Identical lithologic sequences of the same age in UDMA and AAMB suggest that the two belts originally formed a single continental margin magmatic arc that was subsequently rifted apart (Hassanzadeh et al. 2002). Azizi and Jahangiri (2008) stated that the AAMB is related to the Khoy–Zanjan oceanic subduction beneath the Alborz-Azarbaijan plate and not to the Neo-Tethyan subduction beneath the Iranian plate.

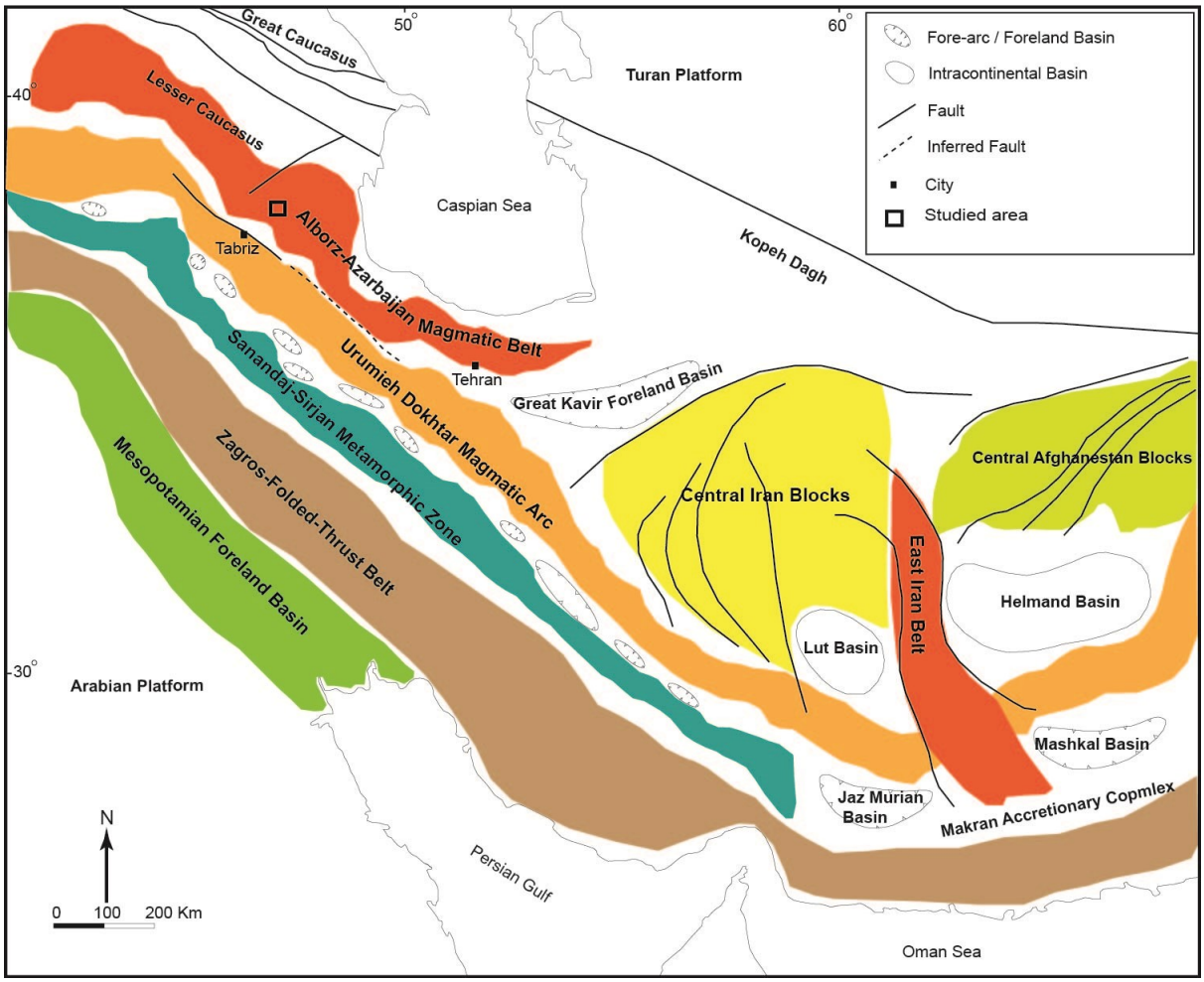

Fig 1. Location of the studied area in the important Iranian structural-magmatic zones (modified from the tectonic map of Middle East, Alavi 1991).

The study area is situated in the AAMB (Fig 1) and placed on the 1/100000 geological map of Khoja. Pre-Cretaceous age rocks are scarce in the NW of Iran including Ahar, Kaleybar, Heris, and Meshkinshar areas, and most of the outcrops are Cretaceous and Tertiary successions. The Upper Cretaceous is recognized with different facies in the NW of Iran as follows: the first is characterized by thick detrital sediments (Ayatakhlet basin) and the second is characterized by dominantly calcareous sediments associated with expanded volcanic activity (Qaradagh-Sheyvardagh basin). There exists a shallow marine environment for the deposition of back-reef limestones associated with marl, molasse and conglomerate during the Upper Cretaceous around the basins to the south and the east (Babakhani et al. 1990). According to Omidvar

et al. (2016), deposition of the Upper Cretaceous sequences in the NW of Iran is assumed to have occurred in various sedimentary environments including siliciclastic setting, shallow carbonate platforms, deep-marine fans and pelagic carbonates. The best outcrop of the Ayatakhlet basin sediments is located in the south of Goouradaraq village (Fig 2). The studied sediment is a part of the Ayatakhlet basin and is composed of bluish or geenish grey shale intercalated with thin detritic limestone, siltstone and sandstone. The Goouradaraq sediments are mainly made up of thinly laminated to very thinly bedded, nodular and massive shales. The interbedded siltstones show moderate to abundant bioturbation and are greenish grey in color. The thickness of the siltstones mostly varies from 3 to 5 cm and are harder than the shales.

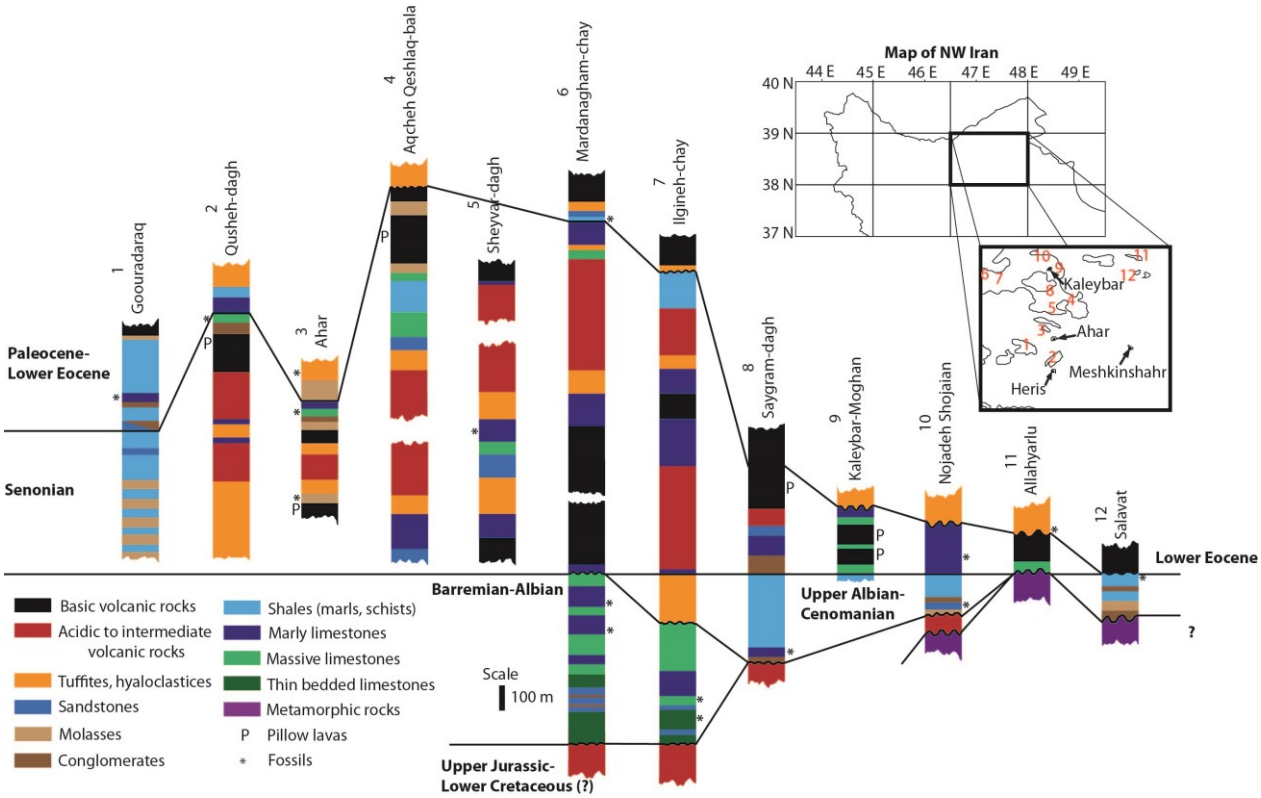

Fig 2. Comparison of the stratigraphic sections of Cretaceous and Paleocene-Lower Eocene in NW Iran (adapted from Babakhani et al. 1990). Index map shows the location of the sections. The first section indicates the stratigraphy of the studied area.

The studied sediments are cut by micro-dioritic dykes and belong to Upper Paleocene based on the existing fossils (Faridi and Hagh Farshi 2006). The studied rocks are in contact with the Paleocene yellowish to bluish grey biomicrosparite limestones, the Eocene pyroclastic and intermediate volcanic rocks, the Miocene red conglomerates and breccias, and the Plio-Quaternary unconsolidated conglomerate interbedded marl. The studied sediments are concordantly placed on the Paleocene limestones. The upper boundary of the sediments is commonly marked by a disconformity or an unconformity surface, covered by the Paleocene-Lower Eocene or Neogene sediments. Commonly, there are reverse and thrust faults in the contacts between the studied rocks and the younger formations (Fig 3).

Pencil cleavage, as a result of intersection between diagenetic and tectonic cleavages, is usually associated with the studied rocks. There is no distinct unconformity between the Cretaceous and Paleogene sediments as a result of the Laramian orogenic phase in the studied section (Babakhani et al. 1990) (Fig 4). Hajalilou et al. (2016) studied Goouydaraq pencil shales (in the vicinity of Goouradaraq village, in this study) and concluded that the Goouydaraq sediments were supplied from the Upper Cretaceous volcanic-sedimentary succession which occurred around the studied area and formed in immature continental magmatic arc of Neo-Tethys.

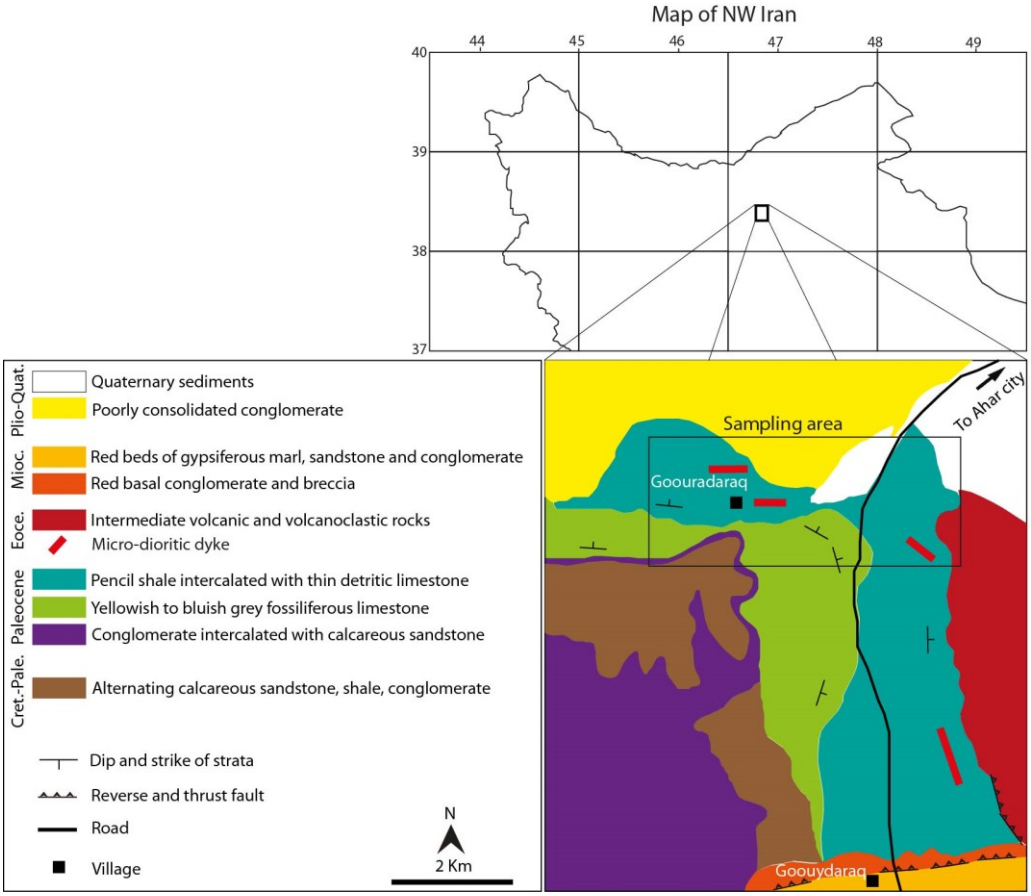

Fig 3. Geological map of the studied area (simplified from Faridi and Hagh Farshi 2006).

3. Materials and Methods

More than twenty samples were collected from the Goouradaraq shale, siltstone, and limestone. The mineralogy and petrography were investigated by polarized-light microscopy of thin sections. Four whole rock powder samples of appropriate shales as random and oriented mounts were analyzed by XRD at the Geological Survey of Iran, Tabriz Center. XRD analyses were carried out using a Siemens D-5000 instrument with Cu-Ka radiation. The samples were saturated with potassium (K) and magnesium (Mg), solvated by ethylene-glycol and heated to 550˚C to distinguish the expandable clay phases. The analytical results are presented in Table 1.

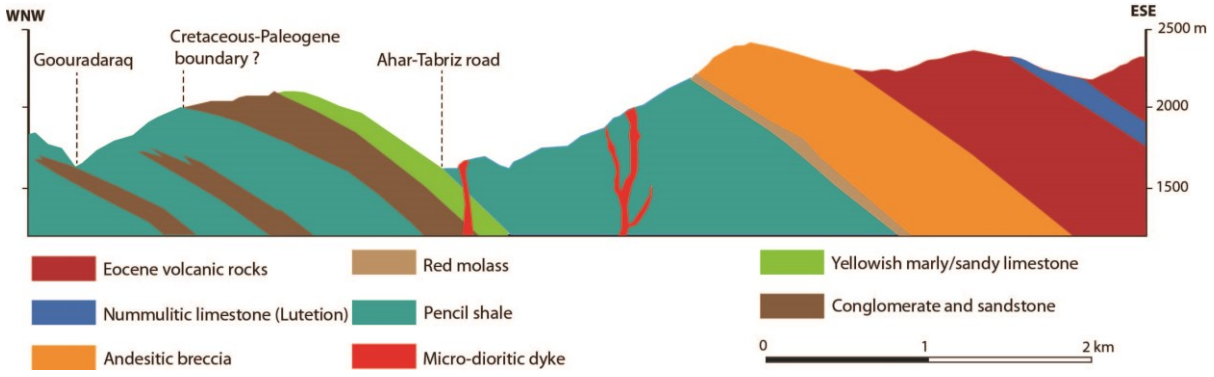

Fig 4. The schematic cross section of Cretaceous (?)-Paleocene-lower Eocene successions in the studied area (modified from Babakhani et al. 1990). The studied sediments are shown as pencil shale.

Representative gold-coated clay-rich samples were used for scanning electron microscope (SEM) and energy dispersive X-ray (EDX), analysis was conduct at the Mechanical Engineering Faculty of Tabriz University with an LEO-440i scanning electron microscope. For major element analysis, whole-rock powders of five samples were fused with $Li_2B_4O_7$ and analyzed on fused discs by using an X-ray fluorescence spectrometer (XRF) at the Kansaran Binaloud Company lab (Iran). The analytical results are presented in Table 2. Trace elements, including rare-earth elements (REE), were determined by an inductively coupled plasma-mass spectrometer (ICP-MS) at the same lab. The analytical results of the three samples are presented in Table 3.

Table 1. XRD analytical results of the Goouradaraq shale including type and percentage of minerals in the samples. Abbreviation symbols are Ch, Chlorite; Il, Illite; Ko, Koninckite; Mm, montmorillonite; Pa, Palygorskite.

Sample no.	Calcite	Quartz	Feldspar	Dolomite	Muscovite	Hematite	Mg-Hornblende	Clay mineral	Clay mineral type
NA-257-14	65	11	4	8	4	-	-	7	Ch, Il, Pa, Mm
NA-245-2	63	20	7	-	2	1	-	6	Ch, Il, Mm
NA-249-6a	65	21	2	-	4	1	-	6	Ch, Il, Mm, Ko
NA-253-10	55	18	7	6	3	-	5	5	Ch, Il, Pa

Table 2. Major element oxides of the studied shale analyzed by XRF, as well some important geochemical parameters.

	NA-253-10	NA-249-6	NA-246-2	NA-244-1	NA-251-8
SiO_2	45.82	42.36	43.01	44.72	43.01
Al_2O_3	13.45	12.99	11.42	12.67	12.76
$Fe_2O_{3(t)}$	5.02	4.69	4.38	4.21	4.69
CaO	15.12	16.94	18.24	15.79	16.52
Na_2O	0.69	0.61	0.64	0.73	0.73
K_2O	3.00	2.93	2.22	2.72	2.87
MgO	1.88	2.29	2.08	2.20	2.37
TiO_2	0.621	0.59	0.567	0.614	0.609
MnO	0.057	0.055	0.069	0.067	0.054
P_2O_5	0.142	0.169	0.147	0.15	0.157
S	0.009	0.027	0.011	0.023	0.013
LOI	13.99	16.21	17.02	15.87	16.03
CIA	70.91	71.50	71.70	70.33	69.85
ICV	1.96	2.16	2.47	2.08	2.18
CIW	85.56	86.62	84.43	84.06	84.16
PIA	81.80	83.03	81.07	80.20	80.08
CIW'	92.22	92.83	91.56	91.34	91.40
Al_2O_3/TiO_2	21.66	22.02	20.14	20.64	20.95
[a] DF1	-0.11	0.32	-0.78	0.50	0.48
[b] DF2	1.18	2.44	2.22	2.67	2.73

[a, b] Discrimination Functions 1 and 2 to discriminate provenance signatures (Roser and Korsch 1988).

Table 3. Trace and rare earth elements concentrations in ppm for the studied shale; detection limit of elements are presented in parenthesis.

element	NA-253-10	NA-249-6	NA-246-2	element	NA-253-10	NA-249-6	NA-246-2
Ag (0.1)	1	0.5	0.7	Pr (0.05)	5.38	5.36	5.37
As (0.1)	26.6	6.3	6.2	Rb (1)	105	108	91
Ba (1)	231	335	177	Sb (0.5)	0.7	0.5	<0.5
Be (0.2)	3.7	3.4	1.8	Sc (0.5)	12.6	13.4	15
Bi (0.1)	0.2	0.2	0.2	Se (0.5)	<0.5	<0.5	<0.5
Cd (0.1)	0.2	0.1	0.1	Sm (0.02)	3.77	3.97	4.26
Ce (0.5)	49	49	46	Sn (0.1)	2	2.1	1.8
Co (1)	13.2	13.4	11.7	Sr (1)	320	474	493
Cr (1)	82	77	70	Ta (0.1)	0.5	0.48	0.4
Cs (0.5)	7	7.2	5.2	Tb (0.1)	0.54	0.56	0.64
Cu (1)	21	22	14	Te (0.1)	<0.1	<0.1	<0.1
Dy (0.02)	3.03	3.11	3.48	Th (0.1)	7.19	6.72	6.64
Er (0.05)	1.89	1.93	2.03	Tl (0.1)	0.44	0.41	0.32
Eu (0.1)	0.89	0.95	1.05	Tm (0.1)	0.25	0.24	0.26
Gd (0.05)	3.26	3.52	3.96	U (0.1)	2.1	1.87	1.7
Hf (0.5)	2.38	2.21	2.22	V (1)	129	126	99
In (0.5)	<0.5	<0.5	<0.5	W (1)	1.6	1.6	1.3
La (1)	26	26	23	Y (0.5)	16.2	18.2	20.5
Li (1)	47	46	43	Yb (0.05)	2.1	2	2
Lu (0.1)	0.29	0.28	0.28	Zn (1)	95	92	63
Mo (0.5)	<0.5	<0.5	<0.5	Zr (5)	98	95	86
Nb (1)	8.4	9.2	8.6	[a] Eu/Eu*	0.78	0.78	0.78
Nd (0.5)	20.2	20.7	21.3	[b] (La/Yb)n	8.35	8.76	7.75
Ni (1)	42	45	37	∑REE	116.60	117.62	113.63
Pb (1)	15	14	10				

[a] $Eu/Eu^*=Eu_N/\sqrt{[(Sm_N).(Gd_N)]}$ as Taylor and McLennan (1985) recommended.
[b] Chondrite values for normalizing are from Boynton (1984).

4. Results

4.1. petrography

The shale samples were characterized by very fine-grained texture and mainly composed of carbonate and clay minerals, as well as a lesser amount of fossil allochems (e.g., Globigerina sp. and Discocyclina sp.). The samples did not exhibit any distinct oriented texture. The interbedded siltstones were composed of calcite, quartz (10-15%), clay minerals, chlorite, muscovite, biotite, opaque minerals, plagioclase, and zircon. The siltstones were commonly characterized by mono-crystalline quartz with parallel extinction which could imply a volcanic igneous provenance for the studied rocks. Also, the quartz grains within the siltstones exhibited features of subangular to subrounded, low-sphericity and poor sorting.

4.2. XRD investigations

The bulk samples and the clay fractions were analyzed by XRD. Table 1 present the analyses of samples. Since the intensity of an X-ray diffraction peak is directly proportional to the mineral volume, therefore semi-quantitative estimation of the mineral content were obtained by measurement of the peak areas. All samples consisted of calcite (55-65 %), quartz (11-

21%), clay minerals (5-7%), feldspar (2-7%), muscovite (2-4%), dolomite, hematite and Magnesiohornblende. Clay minerals were composed of chlorite, illite, montmorillonite, palygorskite, and koninckite. A representative XRD pattern of air-dried Mg- and K-saturated, glycol-treated and heated samples is shown in Figure 5. Chlorite was identified in all the XRD patterns by its characteristic lines at 14.2 Å, 7.1 Å, 4.72 Å, and 3.55 Å. Chlorite and kaolinite have very different structures and geological occurrences, but are sometimes present in natural mixtures. Chlorite has a basal series of diffraction peaks superimposed or nearly superimposed on the members of the kaolinite (001) series. Kaolinite has reflections based on 7.1 Å, 4.36 Å, and 3.57 Å structure. The distinction between chlorite and kaolinite is most difficult when Fe-rich chlorites are involved. The XRD patterns revealed a basal spacing of 10 Å, 5.02 Å, and 3.34 Å for illite. Montmorillonite is easily identified by comparing diffraction patterns of air-dried, ethylene glycol-solvated and heated preparations. Therefore, montmorillonite was characterized by the (001) peak at about 15 Å, 16.9 Å, and 10 Å. The (001) peak at about 10.5 Å in some of the XRD patterns is probably associated with palygorskite (Moore and Reynolds, 1997).

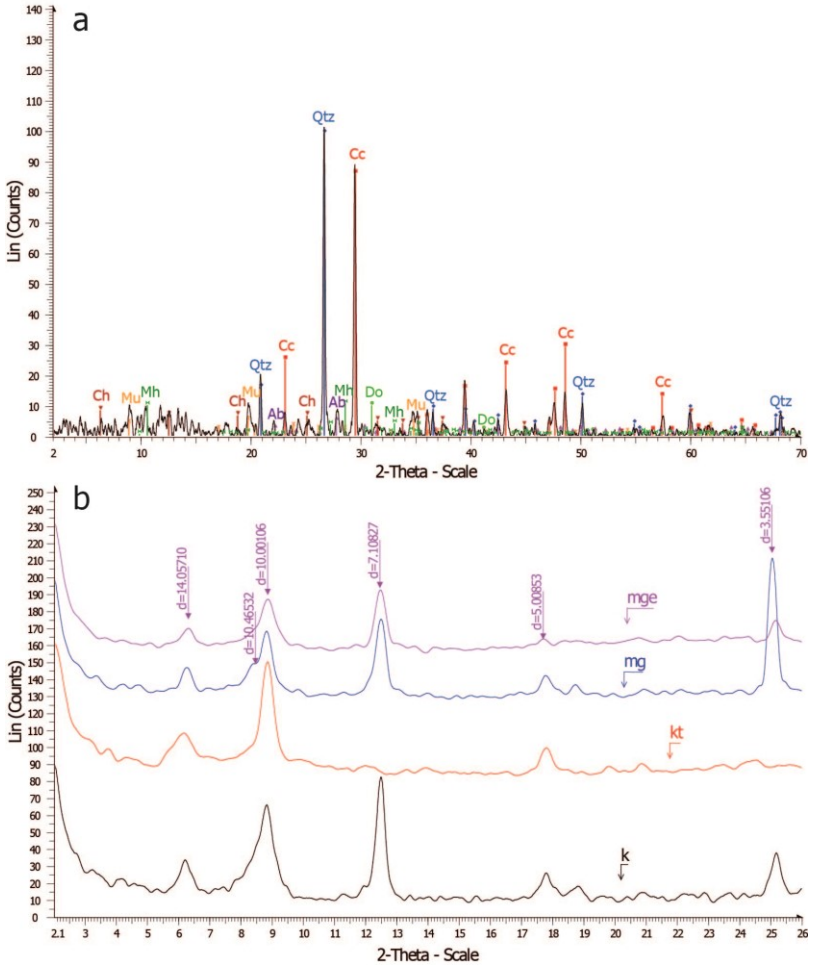

Fig 5. Representative XRD patterns of sample NA-253-10 (a) Qtz, Quartz; Cc, Calcite; Ab, Albite; Ch, Chlorite; Mh, Magnesiohornblende; Do, Dolomite; Mu, Muscovite (b) k, K-saturated; kt, K-saturated and heated at 550˚C; mg, Mg-saturated; mge, treated with Mg and ethylene-glycol.

4.3. SEM observations

The carbonate minerals, including calcite/dolomite, often occur in dissolution cavities as the disseminated and cumulated crystals. Most of the carbonate crystals are subeuhedral, with a spherical or rounded appearance, and are smaller than 2 µm in diameter (Fig 6a). The crystal development of the carbonates was in forms of blades, star-shaped platelets and clusters as illustrated in Figure 6b. Flaky illites were important clay components present in the studied samples. Thin folded flakes of Illite formed oval voids of which some were filled with diagenetic calcite/quartz.

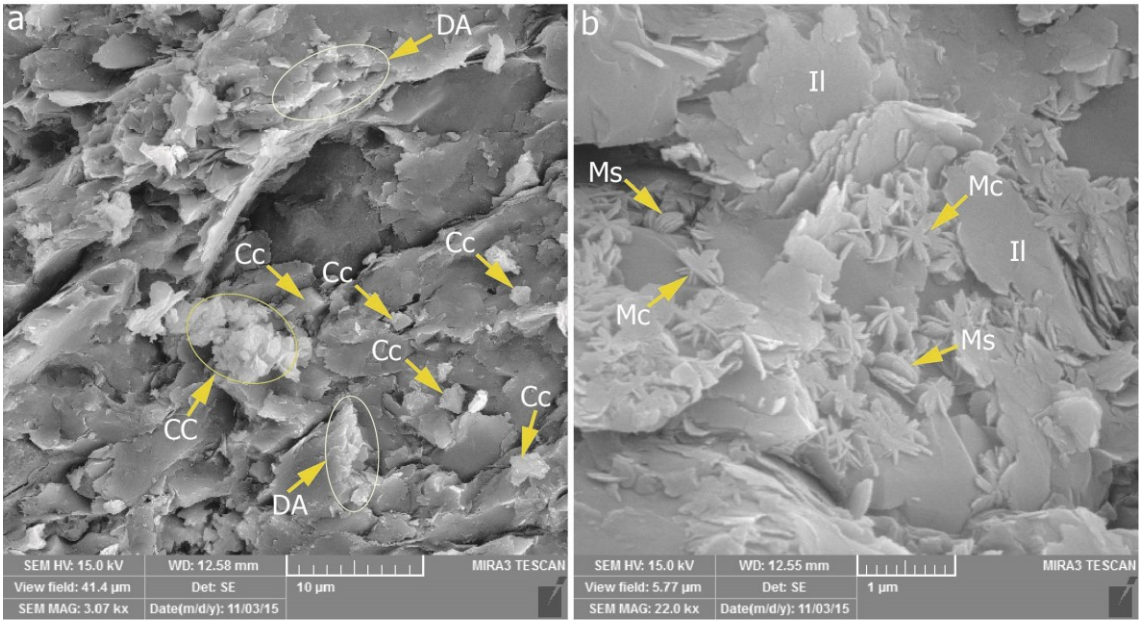

Fig 6. SEM micrographs of the Goouradaraq shale. (a) The cumulated calcite/dolomite (CC), the carbonate minerals (Cc), and dissolution edges in micritic-carbonate (DA). (b) Illite (Il), probable parallel platelets of muscovite (Ms), and star-shaped magnesium carbonate (Mc).

On the surface of illites there are ragged-edged, flaky to crenulated montmorillonite (Fig 7a). Also, illite occurred as thin flakes with ribbon-like projection (Fig 7b, 8b). Dolomite occurred as bladelike crystals near the micritic carbonate grains (Fig 8a). A potential problem in EDX interpretation occurs due to poor resolution and electron beam penetration through very thin materials, such as clays. The electron beam is strong enough to penetrate through a thin mineral into any underlying detrital grain. This gives rise to the weak detection of elements from the underlying grain. Therefore, the studied thin minerals or clays did not show the genuine composite element. The EDX spectrum obtained then represents a composite of both minerals (Welton 2003). Illite EDX analysis revealed the major elements Si, Al, K, and Fe whereas montmorillonite analysis revealed the major elements Si, Al, Ca, Mg and Na. Therefore, the EDX spectrums in Figures 7 and 8b indicate illite and montmorillonite composite. The EDX spectrum in Figure 8a indicates the presence of all the typical major elements of dolomite (Ca, Mg, and Fe) and illite.

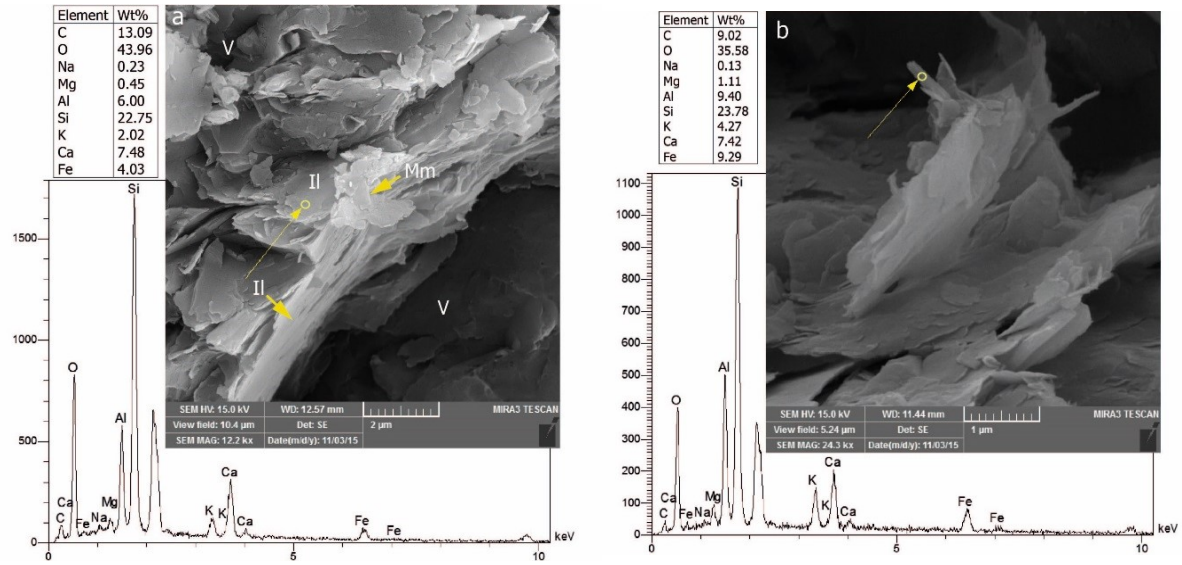

Fig 7. SEM micrographs and EDX analysis of the clay minerals of the studied shale. (a) The thin folded flakes of illite (Il) with ragged-edged and chaotic clusters of montmorillonite (Mm); cavities are represented by letter V. (b) The thin flakes with ribbon-like projections of illite. The yellow circle in the SEM micrographs shows the location of the EDX analysis; the EDX spectrums indicate illite and montmorillonite composite.

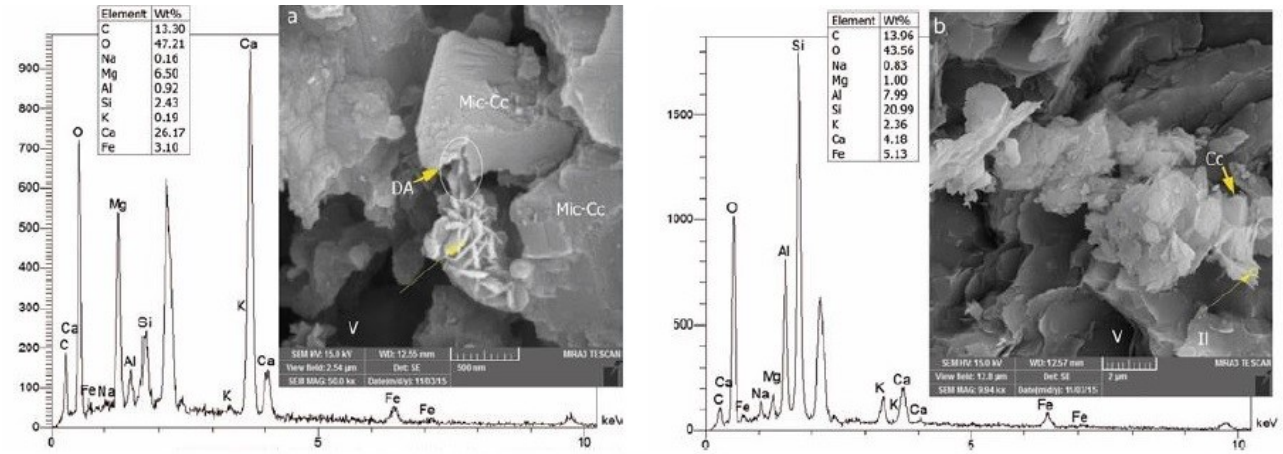

Fig 8. SEM micrographs and EDX analysis of the carbonate and clay minerals of the studied shale. (a) Micritic carbonate grains (Mic-Cc) with dissolution edges (DA); the EDX spectrum indicates dolomite composite. (b) The thin flakes with ribbon-like projections of illite (location of the EDX analysis); the EDX spectrum indicates illite and montmorillonite composite. Abbreviations are the same as in Figures 6 and 7.

4.4. Geochemical properties

4.4.1. Major and trace elements

The concentrations of major and trace elements of the studied samples are listed in Tables 2 and 3. Geochemical classification of the study samples according to the diagram of Herron (1988), log (SiO_2/Al_2O_3) versus log (Fe_2O_3/K_2O), indicates shale composition (Fig 9).

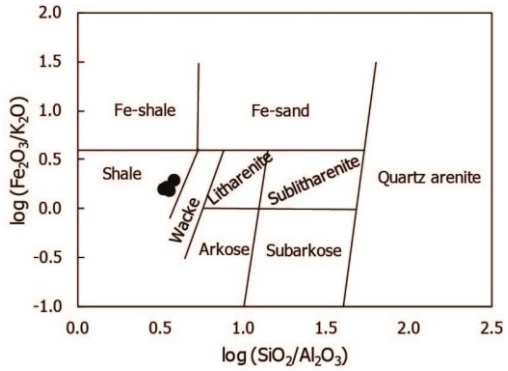

Fig 9. (a) Classification of the GG shale based on the diagram of Herron (1988), log (SiO_2/Al_2O_3) versus log (Fe_2O_3/K_2O).

The CaO content of samples varied from 15.12 to 18.24 and on the average they had higher CaO content in comparison to the Archean Shales (AS), post-Archean Australian Shales (PAAS), and North American Shale Composite (NASC). However, the Goouradaraq shale samples had lower contents of Al_2O_3, SiO_2, and Fe_2O_3 in comparison to the standard shales (Fig 10a). The Cs and Sr content of samples varied from 5.2 to 7.2 and 320 to 493 ppm, respectively which had higher contents in comparison to the NASC, AS, PAAS and Upper Continental Crust (Fig 10b). Other trace elements such as Ba, Nb, Ta, Hf, and Zr had lower contents than the standard samples and Upper Continental Crust.

4.4.2. Rare earth elements

Of the trace elements, the most valuable in geochemistry are the rare earth elements (REE), because they are not fractionated from each other by most sedimentary processes. REE concentrations of the three samples of the studied shales are shown in Table 3.

A chondrite-normalized (Boynton 1984) REE diagram for the studied shale was compared with Chondrite-normalized REE patterns of the orogenic andesites from various tectonic settings (Fig 11a). The REE pattern of the shale exhibited high LREE/HREE, $(La/Yb)_N$ =8.29, and Eu anomaly, Eu/Eu*=0.78. The mean total REE content of the Goouradaraq shale is lower, compared to the standard sediments such as PAAS, NASC, and AS (∑REE=115.95 ppm). Figure 11a also indicates that the REE pattern of the studied shale is similar to that of the Andean-type andesite, especially in the LREE segment. The NASC-normalized REE pattern of Goouradaraq shale was compared with that of mudstones from various tectonic settings including back-arc, continental arc, fore-arc, and strike-slip basins (Fig 11b). According to Figure 11b, the REE profiles are similar except for severe LREE depletion in the Fore-arc basins. Also, the Goouradaraq shale profile indicates HREE enrichment in comparison to back-arc, continental arc, and strike-slip basins profiles.

4.5. Source rocks and tectonic setting

Roser and Korsch (1988) proposed a provenance discrimination diagram. The diagram is widely used to discriminate between primarily mafic, intermediate or felsic igneous and quartzose sedimentary provenances. The discrimination functions are based upon the ratios of TiO_2, $Fe_2O_{3\ (t)}$, MgO, Na_2O, and K_2O all to Al_2O_3 (Fig 12).

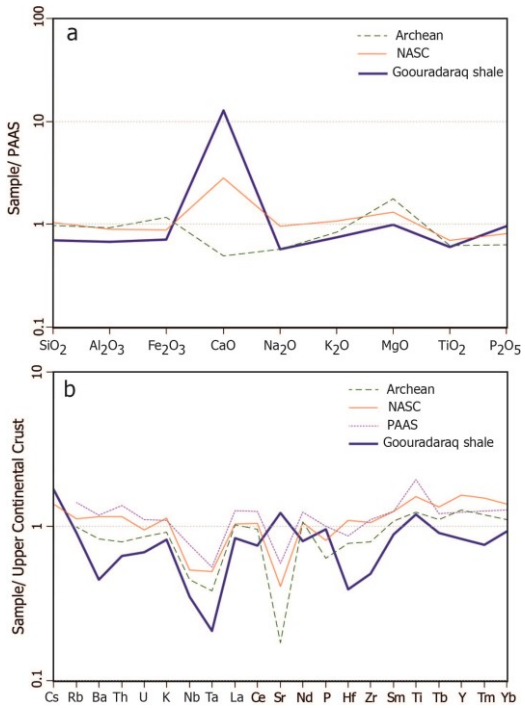

Fig 10. (a) PAAS normalized major oxides for the studied shales compared with NASC and AS; the normalized and compared data are from Condie (1993); (b) the pattern of Upper Continental Crust normalized trace elements for the studied shales compared with PAAS, NASC and AS.

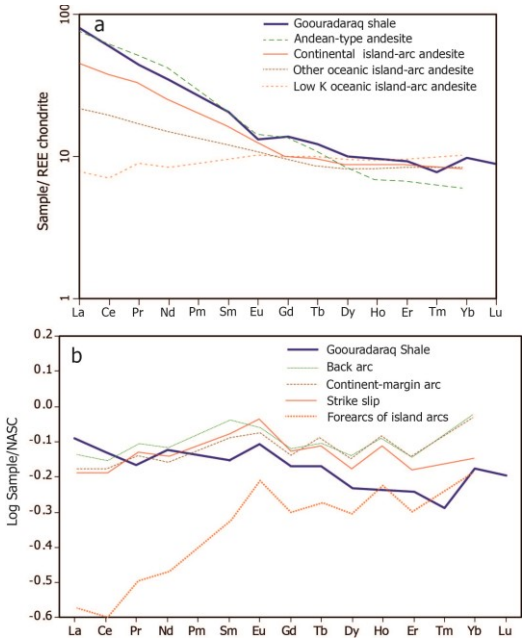

Fig 11. (a) Comparison of chondrite normalized REE patterns of the Goouradaraq shale and various orogenic andesites (Bhatia, 1985). (b) REE patterns for muds from various tectonic settings (McLenann et al. 1990) compared with the Goouradaraq shale. The values of REE for the NASC are from Condie (1993) and Gromet et al. (1984) and for chondrite are from Boynton (1984).

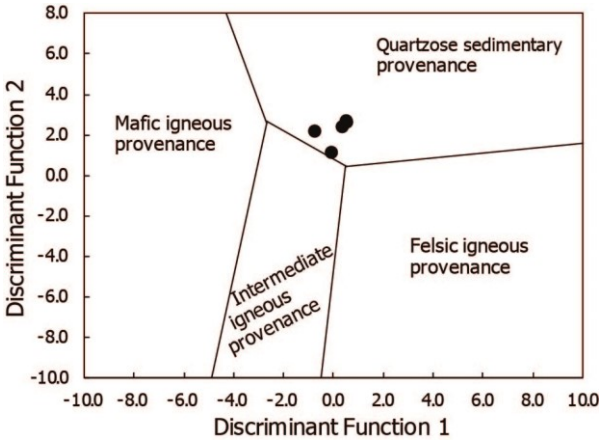

Fig 12. Plot of discrimination scores along Function 1 versus Function 2 diagram (Roser and Korsch 1988) used to discriminate the provenance signatures of the Goouradaraq shale; Discrimination Function 1: 30.638 TiO_2/Al_2O_3 – 12.541 $Fe_2O_{3\ (t)}/Al_2O_3$ + 7.329 MgO/Al_2O_3 + 12.031 Na_2O/Al_2O_3 + 35.402 K_2O/Al_2O_3 – 6.382, Discrimination Function 2: 56.500 TiO_2/Al_2O_3 – 10.879 $Fe_2O_{3(t)}/Al_2O_3$ + 30.875 MgO/Al_2O_3 – 5.404 Na_2O/Al_2O_3 + 11.112 K_2O/Al_2O_3 – 3.89.

All the samples were plotted in quartzose sedimentary field; however, they are near the intermediate igneous field. The concentrations of Na, K, Ca and Mg are enriched/depleted by weathering, transportation from the source rock to the depositional site and diagenesis, whereas Ti, Al, Zr remain unaffected because of low solubility of their oxides and hydroxides in low temperature aqueous solutions (Stumm and Morgan 1981; Sugitani et al. 1996; Hayashi et al. 1997; El-Bialy 2013; Abedini and Calagari 2014). The ratio of Al_2O_3/TiO_2 in shales is similar to that of the parent rocks (Hayashi et al. 1997). Therefore, the Al_2O_3/TiO_2 ratio is used as a significant indicator of source rocks compared to other major oxides. The Al_2O_3/TiO_2 ratios of the Goouradaraq shales ranged from 20.14 to 22.02 (Table 2). Most of the samples exhibited higher Al_2O_3/TiO_2 values (≈21), corresponding to felsic (and/or intermediate) source rocks (Hayashi et al. 1997).

The range of elemental ratios such as Th/Co=0.50-0.57, La/Co=1.94-1.97, Th/Sc=0.44-0.57, La/Sc=1.53-2.06, and Th/Cr=0.09 for the studied samples in comparison to those of the silicic/felsic, intermediate, and basic/mafic sources further strengthened the predominance of felsic/silicic sources for the Goouradaraq shale (Table 4).

The Ti/Zr ratio generally decreases with increasing SiO_2 content, from >200 for mafic igneous rocks, 195-55 for intermediate igneous rocks, to <55 for felsic igneous rocks (Hayashi et al. 1997).

Table 4. The mean values of elemental ratios from the Goouradaraq shale are compared with fine fractions from silicic and basic source rocks. Data were obtained from Cullers and Podkovyrov (2002) and Cullers (2000).

Elemental ratio	Range of fine fractions from silicic sources	Range of fine fractions from basic sources	Goouradaraq shale
La/Sc	0.7-27.7	0.40-1.1	1.53-2.06
Th/Sc	0.64-18.1	0.05-0.4	0.44-0.57
La/Co	1.4-22.4	-	1.94-1.97
Th/Co	0.30-7.5	-	0.50-0.57
Th/Cr	0.067-4.0	0.002-0.045	0.09
Eu/Eu*	0.32-0.83	0.70-1.02	0.78

The Ti/Zr ratio of the Goouradaraq shale ranged from 37 to 39, thus suggesting that the source area was dominated by felsic igneous rocks.

The major and trace element geochemistry of detrital sedimentary rocks can be used to infer provenance type. Also, it will be a useful tool to understanding the tectonic setting of ancient sedimentary basins (Bhatia 1983; Bhatia and Crook 1986). A plot involving $Fe_2O_{3\,(t)}$+MgO versus TiO_2 is used to discriminate between shales deposited in passive margin, active continental margin, continental island arc and oceanic island arc settings (Bhatia 1983). It was discovered from this plot (Fig 13a) that all the Goouradaraq shale samples were plotted in continental arc setting field. Meanwhile, the content of trace elements (Th=6.85 and La=25 ppm) as well as the elemental ratios (Ti/Zr=39, Th/Sc=0.50, La/Sc=1.85, and La/Th=3.6) suggest a continental arc setting for the Goouradaraq shale (Table 5). Also, the ternary diagram of Th-Sc-Zr/10 (Batia and Crook 1986) showed that all the Goouradarq shales were plotted within the continental island arc field (Fig 13b).

Table 5. The comparison of trace and rare earth elements characteristics of the Goouradaraq shale with graywakes and mudrocks from various tectonic settings, as well as some geochemical parameters (Bhatia 1985; Bhatia and Crook 1986); Mean ratios and contents were obtained from three samples.

Element ppm/ Elemental ratio	Oceanic island arc	Continental island arc	Active continental margins	Passive margins	Goouradaraq Shale
Zr/Th	48	-	9.5	-	13.6
Th/U	2.1	-	-	-	3.6
La/Y	0.5	-	-	-	1.4
Ti/Zr	57	20	15	6.7	39
Th/Sc	4.3	0.85	2.6	3.1	0.50
La/Sc	-	1.8	4.5	6.2	1.8
La/Th	-	2.3	1.7	-	3.6
La	8±1.7	27±4.5	37	39	25
Ce	19±3.7	59±8.2	78	85	48
∑REE	58±10	146±20	186	210	116
La/Yb	4.2±1.3	11±3.6	12.5	15.9	12.3
$(La/Yb)_N$	2.8±0.9	7.5±2.5	8.5	10.8	8.3
∑LREE/∑HREE	3.8±0.9	7.7±1.7	9.1	8.5	8.9
Eu/Eu*	1.04±0.11	0.79±0.13	0.60	0.56	0.78

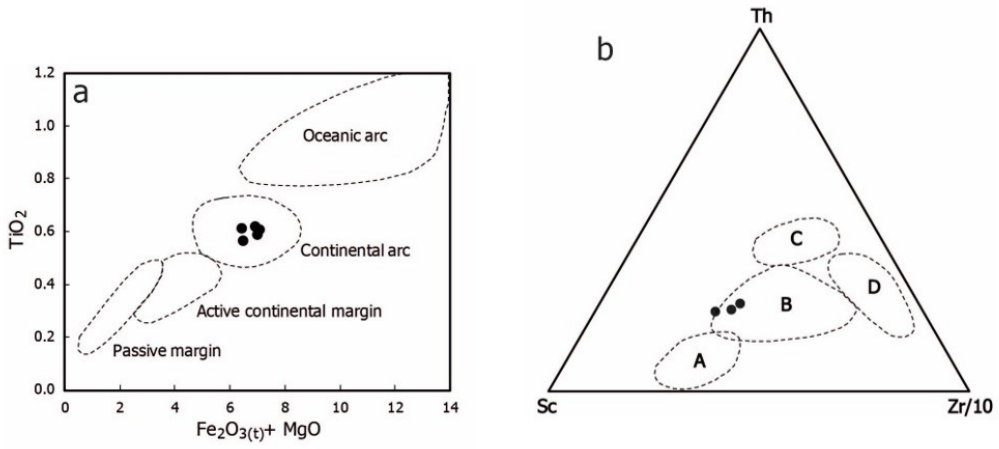

Fig 13. Major and trace element composition plots of the Goouradaraq shale for tectonic setting discrimination. (a) Plot of $Fe_2O_{3\,(t)}$ + MgO versus TiO_2 (Bhatia 1983). $Fe_2O_{3\,(t)}$ represents total iron; (b) Th-Sc-Zr/10 diagram (Batia and Crook 1986) for discrimination of various tectonic settings, A: Oceanic island arc; B: Continental island arc; C: Active continental margins; D: Passive margins.

4.6. Paleoweathering conditions in the provenance

There are various parameters for determining source rock weathering. The Chemical Index of Alteration (CIA) values and A–CN–K compositional space are reliable indicators of paleoweathering and tectonic history of sedimentary rocks. The CIA was proposed by Nesbitt and Young (1982, 1984) as a way of investigating the intensity of chemical weathering in a source area.

$CIA= [Al_2O_3/ (Al_2O_3+CaO^*+K_2O+Na_2O)] \times 100$

Values are expressed as molar proportions and CaO* represents the CaO present in silicate minerals only. The CaO* concentration was calculated based on McLennan (1993). CIA values for the samples varied from 69.85 to 71.70 (Table 2) which suggests moderate weathering in the source area.

As K-metasomatism may possibly reduce the CIA values, many researchers used Plagioclase Index of Alteration, $PIA= [(Al_2O_3-K_2O)/ (Al_2O_3-K_2O+CaO^*+Na_2O)] \times 100$, and Chemical Index of Weathering, $CIW= [Al_2O_3/ (Al_2O_3+CaO^*+Na_2O)] \times 100$, for better estimation of weathering conditions in the source rocks (e.g., Fedo et al. 1995; Harnois 1988). The PIA and CIW values for the Goouradaraq shale ranged from 80.08 to 83.03 and 84.06 to 86.62, respectively (Table 2). Samples that vary a lot in CaO due to variation in calcite may suggest misleading conclusions if the CIW and CIA are used to infer the degree of weathering. Therefore $CIW'= [Al_2O_3/ (Al_2O_3+Na_2O)] \times 100$ could be useful (Cullers, 2000). CIW' values for the samples varied from 91.34 to 92.83 (Table 2). The data indicate a greater degree of weathering of source rocks than the degree of weathering inferred from their CIA values. As interpreted from the CIA discussion, the PIA and CIW data for the shales also support a moderate degree of weathering of the source rocks.

The Index of Compositional Variability, $ICV= (Fe_2O_3+K_2O+Na_2O+CaO+MgO+TiO_2)/ Al_2O_3$, may be used to evaluate the original composition of shales and siltstones (Cox et al. 1995). The non-clay minerals in the original rocks have higher values of ICV than the clay minerals. In relatively unaltered shales and siltstones, composed mostly of feldspar, pyroxene, amphibole, or biotite with less abundant clay minerals, ICV value tend to be greater than one. The ICV values for the Goouradaraq shale ranged from 1.96 to 2.47.

Weathering, as well as post-depositional diagenetic history of clastic sediments can be evaluated by plotting the CIA values in A–CN–K compositional space (Fig 14). In A–CN– K compositional space (A = Al_2O_3, CN = $CaO+Na_2O$, K= K_2O) the oxides are represented in molar proportions (Nesbitt and Young 1984, 1989; Nesbitt et al. 1997; Young and Nesbitt 1999; Nesbitt 2003). In this diagram, during the initial stages of weathering the trends are parallel to the A–CN line, because during that stage Na and Ca are removed with destruction of plagioclase feldspars (a solid arrow starting from the gabbro composition in Figure 14). As weathering continues, K-feldspars are destroyed thereby releasing K and shifting the residual composition towards Al_2O_3. None of the plot samples was near the Al_2O_3-K_2O joins, indicating that severe weathering conditions did not exist in the source area (Hessler and Lowe 2006). An additional advantage of the A–CN–K compositional space is that the estimation of source rock condition is possible by backward projection of the weathered samples to a point on the feldspar join. The regression line through the data points and parallel to the A–CN join is extended back to the plagioclase–K-feldspar join (dashed line in Figure 14). The position of the intersection point, which provides an approximate thought of plagioclase: K-feldspar ratio of the source rock, suggested an intermediate to felsic source for the Goouradaraq shale.

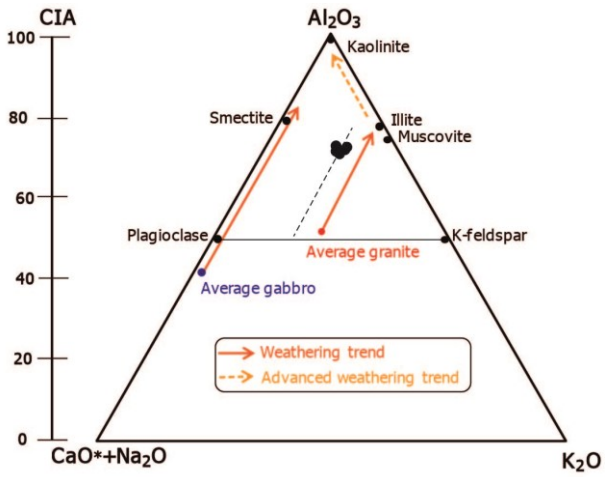

Fig 14. Al_2O_3-($CaO+Na_2O$)-K_2O diagram and CIA (chemical index of alteration) for evaluation of the weathering trend of the Goouradaraq shale. Arrows show the predicted weathering trend of some references compositions including gabbro and granite. The diagram also represents the fields of idealized minerals (Nesbitt and Young 1984, 1989; Fedo et al. 1995).

5. Discussion

Clay mineralogy is considered to be a powerful tool for interpreting weathering conditions and palaeoclimate (Chamley 1989; Ruffell et al. 2002; Sheldon and Tabor 2009), and clay mineral assemblages may provide integrated records of overall climatic impacts (Thiry 2000). In general, illite and chlorite are formed during the initial stages of chemical weathering (Nesbitt et al. 1980; Nesbitt and Young 1989). Their dominance in a sample indicates relatively fast erosion of the source area (Fürsich et al. 2005) and also cold and/or dry conditions. Changes in the clay mineralogy during diagenesis take place principally through the rise in temperature accompanying increased depth of burial.

Passing into the realm of incipient metamorphism, clay minerals are further altered and replaced. Smectites, mixed-layer clays and kaolinite do not survive metamorphism, whereas illite and chlorite continue to exist. Also, illite is replaced by sericite, a finely crystalline variety of muscovite, into the realm of metamorphism (Tucker, 2001). Based on the mineralogy of the Goouradaraq shale, especially the occurrence of chlorite, illite, and muscovite, it assumed that the studied sediments very slightly underwent incipient metamorphism.

The major oxide ratios suggest a quartzose sedimentary and/or intermediate igneous provenance for the studied shale (Fig 12). The Al_2O_3/TiO_2 ratios suggest a felsic (and/or intermediate) source for the Goouradaraq sediments. The range of elemental ratios such as Th/Co, La/Co, Th/Sc, La/Sc, Th/Cr and Ti/Zr for the studied samples in comparison to those of the silicic/felsic, intermediate, and basic/mafic sources (Hayashi 1997; Cullers 2000; Cullers and Podkovyrov 2002), as well as the chondrite normalized LREE patterns, further strengthen the predominance of felsic and intermediate sources for the Goouradaraq shale. The chondrite normalized REE pattern of the Goouradaraq shale is similar to the pattern of Andean-type andesite which probably points to an intermediate igneous source.

The A– CN–K compositional space for the Goouradaraq shales provides valuable information regarding paleoweathering, paleotectonics and source rock composition. The A– CN–K diagram suggests that severe weathering conditions did not exist in the source area and the source rock was an intermediate to felsic igneous rock. Also PIA, CIA and CIW suggest moderate climatic conditions during deposition and indicate that extreme weathering conditions were probably negligible in the source area. Shales and siltstones with ICV's greater than one are most likely first cycle sediments, and those with ICV's less than one may be recycled or intensely weathered first cycle sediment. The ICV values for the Goouradaraq shale are greater than one. Such shales and siltstones are usually deposited as first cycle deposits in technically active areas (Pettijohn et al. 1987; Van de Kamp and Leake 1985; Cullers and Podkovyrov, 2002). Meanwhile, shales and siltstones with scarce clay minerals tend to have ICV's greater than one and are formed in areas of most uplift and are not associated with extensive chemical weathering (Cox et al. 1995).

The elemental ratios value and the rare earth element concentrations including Th/Sc=0.5, Ti/Zr=39, La/Sc= 1.8, La=25 ppm, and Ce=48 ppm, as well as the geochemical parameters such as ∑REE=116, Eu/Eu*=0.78, and $(La/Yb)_N$=8.3 all suggest a continental arc setting for the Goouradaraq shale (Table 4). Also the NASC-normalized REE profiles (Fig 11b) showed that the studied sediments are unrelated to fore-arc basins which have severe LREE depletion (McLenann et al. 1990). Therefore, they are formed in the back-arc, continental arc, or strike-slip basins.

Geological studies showed that the Neo-Tethys subduction under the Central and NW Iran was active during the Upper Cretaceous to Late Miocene (Berberian 1983; Mollai et al. 2014). Therefore, the thick layers of acidic to intermediate volcanic rocks associated with marl, limestone, sandstone, molasse and basic volcanic rock (Babakhani et al. 1990), could be formed during the Upper Cretaceous to Paleocene in NW Iran (Fig 2). Based on the present findings, it was inferred that the studied sediments were more probably supplied from the above volcanic-sedimentary succession. However, geochemical investigations on the interbedded siltstones are obligatory to verify the source rocks.

6. Conclusions

The mineralogical composition and the average values of weathering indices (CIA=71, CIW=85, CIW'=92 and PIA=81), as well as the ICV values (≈2) imply less abundant clay minerals in the studied sediments, moderate weathering in the source area, and deposition as first cycle sediments in an area of relatively high uplift. The values of Al_2O_3/TiO_2, Th/Co, La/Co, Th/Sc, La/Sc and Th/Cr further strengthen the predominance of felsic and/or intermediate sources for the studied sediments. Moreover, the value of the elemental ratios the rare earth element concentrations suggest a continental arc or back-arc setting for the Goouradaraq sediments. Therefore, the source rocks for the Goouradaraq sediments were most probably the Upper Cretaceous succession formed by the Khoy–Zanjan oceanic subduction beneath the Alborz-Azarbaijan plate or the Neo-Tethyan subduction beneath the Iranian plate during the Upper Cretaceous to Paleogene.

Acknowledgments

This work was financially supported by the Research Bureau of the Payame Noor University (Iran), for which we are thankful. The authors would like to acknowledge contributions of the IJES reviewers in improving the manuscript by providing valuable suggestions.

References

Abedini A, Calagari AA (2014) REE geochemical characteristics of titanium-rich bauxites: the Permian Kanigorgeh horizon, NW Iran, *Turkish Journal of Earth Sciences* 23:513-532.

Alavi M (1991) Tectonic Map of the Middle East, 1/5000000, Geological Survey of Iran.

Alavi M (2004) Regional stratigraphy of the Zagros folded-thrust belt of Iran and its proforeland evolution, *American Journal of Science* 304:1–20.

Azizi H, Jahangiri A (2008) Cretaceous subduction-related volcanism in the northern Sanandaj-Sirjan Zone, Iran, *Journal of Geodynamics* 45:178–190.

Babakhani AR, Lesquyer JL, Riou R (1990) Geological Map of Ahar Quadrangle (scale 1:250,000), Geological Survey of Iran, Tehran, Iran.

Berberian M (1983) The southern Caspian: A compressional depression floored by a trapped, modified oceanic crust, *Canadian Journal of Earth Sciences* 20:163-183.

Bhatia MR (1983) Plate tectonics and geochemical composition of sandstones, *Journal of Geology* 91:611–627.

Bhatia MR, Crook KAW (1986) Trace element characteristics of greywackes and tectonic setting discrimination of sedimentary basins, *Contributions to Mineralogy and Petrology* 92:18l- 193.

Blatt H (1985) Provenance studies and mudrocks, *Journal of Sedimentary Petrology* 55:69–75.

Boynton WV (1984) Geochemistry of rare earth elements: meteorite studies, In: Henderson P (Ed.) Rare Earth Element Geochemistry. Elsevier, New York 63-114 pp.

Cao J, Wu M, Chen Y, Hu K, Bian L, Wang L, Zhang Y (2012) Trace and rare earth element geochemistry of Jurassic mudstones in the northern Qaidam Basin, northwest China, *Chemie der Erde Geochemistry* 72:245-252.

Chamley H (1989) Clay Sedimentology. Springer Verlag 623 p.

Condie KC (1991) Another look at rare earth elements in shales, *Geochimica et Cosmochimica Acta* 55:2527–2531.

Condie KC (1993) Chemical composition and evolution of the Upper continental crust: contrasting results from surface samples and shales, *Chemical Geology* 104:1–37.

Cox R, Lowe DR, Cullers RL (1995) The influence of sediment recycling and basement composition of evolution of mudrock chemistry in the southwestern United States, *Geochimica et Cosmochimica Acta* 59:2919–2940.

Cullers RL (2000) The geochemistry of shales, siltstones and sandstones of Pennsylvanian-Permian age, Colorado, USA: Implications for provenance and metamorphic studies. *Lithos* 51:181–203.

Cullers RL, Barrett T, Carlson R, Robinson B (1987) Rare-earth element and mineralogic changes in Holocene soil and stream sediment: a case study in the Wet Mountains, Colorado, USA, *Chemical Geology* 63:275–297.

Cullers RL, Basu A, Suttner L (1988) Geochemical signature of provenance in sand-size material in soils and stream sediments near the Tobacco Root batholith, Montana, USA, *Chemical Geology* 70:335–348.

Cullers RL, Podkovyrov VM (2002) The source and origin of terrigenous sedimentary rocks in the Mesoproterozoic Ui group, southeastern Russia, *Precambrian Research* 117:157–183.

Dewey JF, Pitman WC, Ryan WBF, Bonnin J (1973) Plate tectonics and the evolution of the Alpine System, *Geological Society of America Bulletin* 84: 3137–3180.

El-Bialy MZ (2013) Geochemistry of the Neoproterozoic metasediments of Malhaq and Um Zariq formations, Kid metamorphic complex, Sinai, Egypt: implications for sourcearea weathering, provenance, recycling, and depositional tectonic setting, *Lithos* 175:68-85.

Faridi M, Hagh Farshi E (2006) Geological map of Khoja (scale 1/100,000). Geological Survey of Iran, Tehran, Iran.

Fedo CM, Eriksson KA, Krogstad EJ (1996) Geochemistry of shales from the Archean (~3.0 Ga) Buhwa Greenstone Belt, Zimbabwe: implications of provenance and source-area weathering, *Geochimica et Cosmochimica Acta* 60:1751–1763.

Fedo CM, Nesbitt HW, Young GM (1995) Unraveling the effects of K-metasomatism in sedimentary rocks and paleosols, with implications for paleoweathering conditions and provenance, *Geology* 23:921–924.

Fleet AJ (1984) Aqueous and sedimentary geochemistry of the rare earth elements. In Henderson P (ed.) Rare earth element geochemistry, *Elsevier* 343-373 pp.

Fürsich FT, Singh IB, Joachimski M, Krumm S, Schlirf M, Schlirf S (2005) Palaeoclimate reconstructions of the Middle Jurassic of Kachchh (western India): an integrated approach based on palaeoecological, oxygen isotopic, and clay mineralogical data. Palaeogeography, Palaeoclimatology, *Palaeoecology* 217:289–309.

Gosh S, Sarkar S (2010) Geochemistry of Permo-Triassic mudstone of the Satpura Gondwana Basin, Central India: clues for provenance, *Chemical Geology* 277:78-100.

Graver JI, Scott TJ (1995) Trace elements in shale as indicators of crustal province and terrain accretion in the southern Canadian Cordillera, *Geological Society of America Bulletin* 107:440–453.

Gromet L.P, Dymek R.F, Haskin L.A and Korotev R.L (1984) The "North American Shale Composite": Its Compilation, Major and Trace Element Characteristics, *Geochimica et Cosmochimica Acta* 48:2469-2482.

Hajalilou B, Ashrafi N, and Sharifi J (2016) Mineralogy and Geochemistry of the Upper Paleocene Shales from Goouydaraq-Goouradaraq, East Azarbaijan, NW Iran, *Open Journal of Geology* 6:1096-1117.

Harnois L (1988) The CIW index: a new chemical index of weathering, *Sedimentary Geology* 55:319–322.

Hassan S, Ishiga H, Roser BP, Dozen K, Naka T (1999) Geochemistry of Permian–Triassic shales in the Salt Range, Pakistan: implications for provenance and tectonism at the Gondwana margin, *Chemical Geology* 158:293–314.

Hassanzadeh J, Ghazi AM, Axen G, Guest B (2002) Oligomiocene mafic-alkaline magmatism north and northwest of Iran: evidence for the separation of the

Alborz from the Urumieh–Dokhtar magmatic arc. Geological Society of America, Abstracts with Programs 34, 331.

Hayashi K, Fujisawa H, Holland HD, Ohmoto H (1997) Geochemistry of ~1.9 Ga sedimentary rocks from northeastern Labrador, Canada, *Geochimica et Cosmochimica Acta* 61:4115–4137.

Herron MM (1988) Geochemical classification of terrigenous sands and shales from core or log data, *Journal of Sedimentary Petrology* 58:820–829.

Hessler AM, Lowe DM (2006) Weathering and sediment generation in the Archean: An integrated study of the evolution of siliciclastic sedimentary rocks of the 3.2 Ga Moodies Group, Barberton Greenstone Belt, South Africa, *Precambrian Research* 151:185–210.

Jackson JA, McKenzie D (1984) Active tectonics of the Alpine–Himalayan belt between western Turkey and Pakistan, *Geophysical Journal of the Royal Astronomical Society (C77)* 185–264.

McLennan SM (1989) Rare earth elements in sedimentary rocks: influence of provenance and sedimentary processes. Mineralogical Society of America, *Reviews in Mineralogy and Geochemistry* 21:169–200.

McLennan SM (1993) Weathering and global denudation, *Journal of Geology* 101:295–303.

McLennan SM, Hemming S, McDaniel DK, Hanson GN (1993) Geochemical approaches to sedimentation, provenance, and tectonics. In: Johnson MJ, Basu A (Eds.), Processes Controlling the Composition of Clastic Sediments. *Geological Society of America, Colorado, Boulder* 21–40.

McLennan SM, Taylor SR, McCulloch MT, Maynard JB (1990) Geochemical and Nd–Sr isotopic composition of deep sea turbidites: Crustal evolution and plate tectonic associations, *Geochimica et Cosmochimica Acta* 54:2015–2050.

Mollai H, Pe-Piper G, Dabiri R (2014) Genetic relationships between skarn ore deposits and magmatic activity in the Ahar region, Western Alborz, NW Iran: Evidence for metasomatism and copper mineralization, *Geologica Carpathica* 65(3): 207 – 225.

Moore DM, Reynolds RC (1997) X-ray diffraction and the identification and analysis of clay minerals. Oxford University Press, 378 p.

Nesbitt HW, Fedo CM, Young GM (1997) Quartz and feldspar stability, steady and non-steady-state weathering and pedogenesis of siliciclastics sands and muds, *Journal of Geology* 105:173–191.

Nesbitt HW, Markovics G, Price RC (1980) Chemical processes affecting alkalis and alkaline earths during continental weathering, *Geochimica et Cosmochimica* Acta 44:1659–1666.

Nesbitt HW, Young GM (1982) Early Proterozoic climates and plate motions inferred from major element chemistry of lutites, *Nature* 299:715–717.

Nesbitt HW, Young GM (1984) Prediction of some weathering trends of plutonic and volcanic rocks based on thermodynamic and kinetic considerations, *Geochimica et Cosmochimica Acta* 48:1523–1534.

Nesbitt HW, Young GM (1989) Formation and diagenesis of weathering profiles, *Journal of Geology* 97:129–147.

Nesbitt HW (2003) Petrogenesis of Siliciclastic Sediments and Sedimentary Rocks. In: Lenz DR (Ed.), Geochemistry of Sediments and Sedimentary Rocks. Geotext 4, Geological Association of Canada, Newfoundland, 39-51.

Omidvar M, Safari A, Vaziri-Moghaddam H, Ghalavand H (2016) Facies analysis and paleoenvironmental reconstruction of Upper Cretaceous sequences in the eastern Para-Tethys Basin, NW Iran, *Geologica Acta* 14:363-384.

Paikaray S, Banerjee S, Mukherji S (2008) Geochemistry of shales from the Paleoproterozoic to Neoproterozoic Vindhyan Supergroup: Implications on provenance, tectonics and paleoweathering, *Journal of Asian Earth Sciences* 32:34–48.

Pettijohn FJ, Potter PE, Siever R (1987) Sand and Sandstone. Springer 553 p.

Rollinson HR (1993) Using Geochemical Data: Evaluation, Presentation, Interpretation. Longman Scientific and Technical, Wiley, New York, 352 p.

Roser BP, Korsch RJ (1988) Provenance signatures of sandstone-mudstone suites determined using discriminant function analysis of major-element data, *Chemical Geology* 67:119–139.

Ruffell A, McKinley JM, Worden RH (2002) Comparison of clay mineral stratigraphy to other proxy palaeoclimate indicators in the Mesozoic of NW Europe, *Philosophical Transactions of the Royal Society, London A* 360:675–693.

Sengor AMC (1984) The Cimmeride orogenic system and tectonics of Eurasia. Geological Society of America, Special Paper, 195 p.

Sheldon ND, Tabor NJ (2009) Quantitative paleoenvironmental and paleoclimatic reconstruction using paleosols, *Earth Science Reviews* 95:1–52.

Stocklin J, Nabavi MH (1973) 1/2500000 sheet, tectonic map of Iran, Geological Survey of Iran.

Stumm W, Morgan JJ (1981) Aquatic Chemistry: An Prologue Emphasizing Chemical Equilibra in Natural Waters. John Wiley and Sons, New York, 780 p.

Sugitani K, Horiuchi Y, Adachi M (1996) Anomalously low Al_2O_3/ TiO_2 values for Archean cherts from the Pilbara block, western Australia – possible evidence for extensive chemical weathering on the early earth, *Precambrian Research* 80:49–76.

Taylor SR, McLennan SM (1985) The Continental Crust: Its Composition and Evolution: An Examination of the Geochemical Record Preserved in Sedimentary Rocks. Blackwell Science, Oxford 312 p.

Taylor SR, McLennan SM (1991) Sedimentary rocks and crustal evolution; tectonic setting and secular trends, *Journal of Geology* 99:1–21.

Thiry M (2000) Palaeoclimatic interpretation of clay minerals in marine deposits: an outlook from the continental origin, *Earth-Science Reviews* 49:201–221.

Tucker ME (2001) Sedimentary Petrology: an Introduction to the Origin of Sedimentary Rocks. Blackwell Science, Oxford 262 p.

Van de Kamp PC, Leake BE (1985) Petrography and geochemistry of feldspathic and mafic sediments of the northeastern Pacific margin, *Transactions of the Royal Society of Edinburgh Earth Sciences* 76:411–449.

Welton JE (2003) SEM petrology atlas. The American Association of Petroleum Geologists 240 p.

Young GM, Nesbitt HW (1999) Paleoclimatology and Provenance of the Glaciogenic Gowganda Formation (Paleoproterozoic), Ontario, Canada: A Chemostratigraphic Approach, *Geological Society of America Bulletin* 111:264-274.